Astron. Astrophys. 328, 641–648 (1997)

ASTRONOMY AND ASTROPHYSICS

A study of the planetary nebula K3-82

W. Saurer⋆

Institut für Astronomie, Leopold-Franzens-Universität, Technikerstr. 25, A-6020 Innsbruck, Austria

Received 24 April 1997 / Accepted 5 August 1997

Abstract. In this paper we present Fabry-Pérot high resolution spectroscopy in Hα, Hβ, [O III], and [N II], optical low resolution spectroscopy spanning the usable range 4700–6800 Å, along with a broad band direct image in Gunn-red for the planetary nebula (PN) K3-82. K3-82 turned out to be highly symmetrical, seen most probably edge-on. Two point-symmetrical knots appear in the light of Gunn-red. These knots either represent concentrated emission regions or are part of an incomplete equatorial waist of K3-82. Our results for the systemic velocity is –62.4±5 km/s and for the average expansion velocity 30±5 km/s. For the distance we determined a minimum value of 2.5 kpc. The [S II] ion indicates a very low density within the knots of K3-82.

Key words: planetary nebulae: individual: K3-82 (PN G093.3−00.9)

1. Introduction

The evolution of stars from the asymptotic giant branch to the white dwarf stages and the associated creation of planetary nebulae (PNe) shells seems to be understood in principle nowadays (for a review see, e.g., Iben 1995). This evolution is believed to be dominated by a fast wind which drives a shock wave into the non-isotropic remnants of a slow wind and leads to a significant density enhancement (Kwok et al. 1978: two-winds model, interacting-winds model, and many subsequent articles, e.g. Mellema et al. 1991, Icke et al. 1992, Frank et al. 1993, Stanghellini et al. 1993, Corradi & Schwarz 1995, Pascoli 1995). Non-isotropic slow winds can be produced both by a rotating single star (Dorfi & Höfner 1996), by binary stars (Livio 1995), and/or in the presence of a toroidal magnetic field (Chevalier 1995).

However, numerous details in that process remain to be analyzed and to be explained both theoretically and observationally. In particular, the surrounding interstellar medium (ISM) can influence the shapes of the PNe shells significantly. On the one hand, these interactions represent a new way to study the ISM. On the other hand, they make it difficult to separate the effects of an undisturbed shell evolution from additional effects. For purposes of classification (e.g. Balick 1987, Manchado et al. 1996) and for investigating intrinsic properties of the shell's evolution (e.g. expansion velocities), PNe for which additional effects due to the ISM can be believed to be minimized should be studied.

K3-82 (PN G093.3–00.9, $\alpha_{2000.0} = 21^{h}30^{m}52^{s}0$, $\delta_{2000.0} = +50°00'09''$) was discovered by Kohoutek (1972). Available observational data can be found in the Strasbourg-ESO Catalogue of Galactic PNe (Acker et al. 1992) This PN appears as a nearly undisturbed geometrical ring on the Palomar Observatory Sky Prints (POSS) which has defied detailed individual investigation until now. Due to the classification scheme of Balick (1987) it would be of early round class according to the POSS.

The aim of this paper is to present new measurements on the PN K3-82 for which the data are very scarce until now, to study its morphological and expansion characteristics, and to make an attempt to determine an individual distance to this PN.

2. Observations

2.1. Direct images

An image taken with the broad band filter Gunn-red (central wavelength/bandwidth 6560/840 Å, 600 sec) was obtained in May 1986 using the 2.2 m telescope on Calar Alto (seeing $\approx 1''.2$) with a RCA (SID501 EX) detector (pixelsize 30 μm, corresponding to $0''.3$ per pixel). Standard reduction was applied using MIDAS.

2.2. Fabry-Pérot high resolution spectroscopy

These observations were carried out in October 1984 and May 1986 with a pressure scanned Fabry-Pérot spectrometer (Hippelein & Münch 1981) attached to the 1.23 m telescope on Calar Alto. The nebula was observed using the interference filters Hβ 4866/11, [O III] 5011/18, Hα 6570/15, and [N II] 6590/20. The integration time was 10 sec for Hα and [O III] and 20 sec

Send offprint requests to: Walter.Saurer@uibk.ac.at

⋆ Visiting Astronomer at the Centro Astronomico Hispano-Aleman, Calar Alto, operated by the Max-Planck-Institut für Astronomie, Heidelberg, jointly with the Spanish National Commission for Astronomy; and at the 1.83 m telescope of the University of Padova, Cima Ekar, Asiago, Italy.

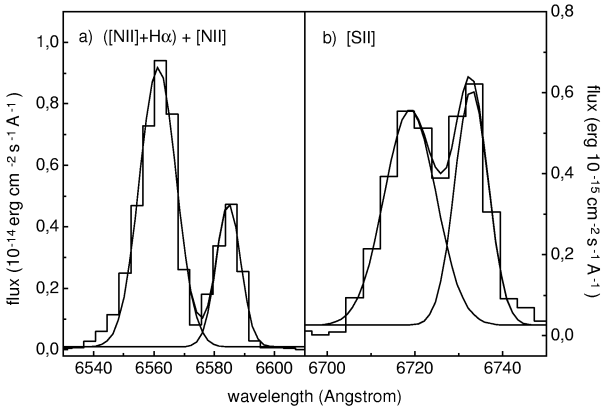

Fig. 1a and b. Two examples showing the line fitting procedure applied for Hα+N[II] and [S II]

for Hβ and [N II] for each data point with a velocity separation of 3.1 km/s, and a spectral resolution of ≈10 km/s. The scans were taken at the center of the nebula with an aperture of 60″ entirely covering the nebula. They were sky subtracted by means of measurements at positions nearby the nebula and corrected for atmospheric extinction. The wavelength calibration was done using laboratory lamps. Absolute flux calibration was carried out using scans of the standard nebulae NGC 6543 and NGC 7027 and the line fluxes as tabulated by Hippelein (1984). Gaussian fittings were performed using the PC program ORIGIN.

2.3. Low resolution spectroscopy

These observations were carried out in January 1997 with the Boller & Chivens spectrograph attached to the 1.83 m telescope of the University of Padova (Cima Ekar, Asiago, Italy). We used a slit width of 250 μm and a grating of 300 lines/mm with a dispersion of 169 Å/mm corresponding to a scale of 3.9 Å/mm. The spectral resolution is ≈10Å (FWHM) and the usable spectral range 4700–6800 Å. The spatial scale is ≈ 1″/pixel which coincides with the spatial resolution (seing ≈ 1″). The detector was a TH 7882 CCD chip with 580×388 pixels (23 μm). For the wavelength calibration we used a FeAr laboratory lamp and absolute calibrations were performed using Hiltner 600 as a standard star. The exposure time was 3 600 sec. Data reduction was carried out with MIDAS (bias, flatfield), IRAF (extraction, sky subtraction), and ORIGIN (line fitting). Examples for the results of the line fitting are presented in Fig. 1.

2.4. Iris measurements

These photographic measurements were carried out with the iris photometer of the institute of Innsbruck (Ebner 1973). We have selected 110 stars with a maximum angular distance of 10′ to K3-82. The plates used were taken with the 1.2 m telescope of Asiago in Johnson U, B, and V. For our measurements we used a total of nine plates, three for every filter. Each star was measured three times on every plate to determine a mean value for one

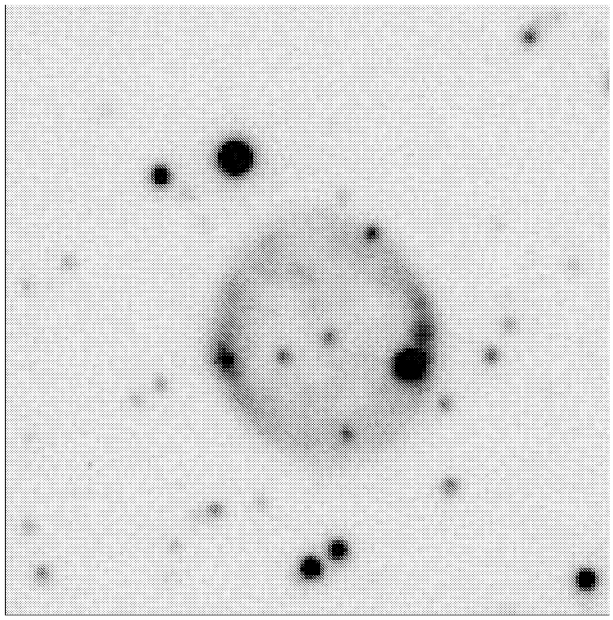

Fig. 2. Direct image of K3-82 in the light of Gunn red. The size of the image is 54″ × 54″, North is to the top and East to the left

plate. Sky subtraction was carried out by means of positions spread over the star fields. The results were averaged for each filter used. For absolute calibrating the data we have made use of 30 stars in NGC 7086 (Hoag et al. 1961) and 17 stars in a star field reported in Saurer et al. (1992), their field IV. All these standard stars are on the same plates as the program stars. The errors of the measurements were determined to be ≈0.06. The measured brightnesses in U, B, and V and a finding chart of all program stars can be found in Table 3 and Fig. 7.

3. Results and discussion

3.1. Morphology

The direct image in Gunn red is presented in Fig. 2. Due to the central wavelength and bandwidth this filter is tracing the PN mainly in the light of Hα+[N II].

From a geometrical point of view K3-82 appears to be a nearly perfect ring with a radius of 10″. The diameter in north-south direction is larger than in east-west direction by only ≈7%. At first glance, from its appearance on the Palomar Observatory Sky Prints, we would expect this PN to be seen almost perfectly pole-on. However, investigating details of its morphology also permits different interpretations.

Two point-symmetrical knots are visible in the east and west of the ring with a position angle (P.A.) of ≈ 97°. Starting from these knots the intensity is decreasing along the ring in north and south direction. It also appears that the ring is somewhat broken in the north. Unfortunately, in the south the emission is contaminated by a star. In addition, even though only slightly, the north-south dimension is larger than the east-west extent. These morphological characteristics are indications that the line-of-

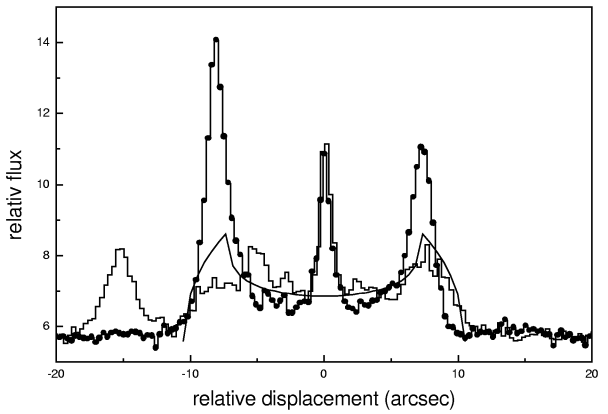

Fig. 3. The relative brightness distribution of K3-82 in the light of Gunn red along a cut through the two knots (P.A. 97° in Fig. 2, histogram with dots) and along the direction perpendicular to that (histogram). From left to right the distributions represent east to west and north to south, respectively. The curve drawn in gives the brightness distribution expected from a sphere with an inner to outer radius ratio of 0.7

sight view to K3-82 can also be edge-on in accordance with the two-winds model.

Fig. 3 shows the relative brightness distributions along a cut through the nebula including the two knots (P.A. 97°, histogram with dots) and along an axis approximately perpendicular (to avoid the contamination by the star in the south) to that (histogram). The curve drawn into Fig. 3 gives the brightness distribution which would be expected from a sphere with an inner to outer radius ratio of 0.7 (estimated from the direct image). From the high ratio of the peak values to the central trough in Fig.3 we can conclude that the two knots do not represent the edge brightened parts of a closed toroidal structure seen edge-on. Either the torus is not closed or the two knots represent additional, highly concentrated features within the shell.

The brightness distribution along the north-south direction is not in contradiction to what is expected from a sphere. This would be more in favour of seeing K3-82 edge-on, as long as the shell of the PN is not an (approximately homogeneously) filled sphere itself. This third possibility, i.e. the PN is neither seen edge-on nor pole-on cannot be ruled out with certainty, however, it would be difficult to explain the point-symmetrical knots.

In summary, our data do not permit to make a final decision on the viewing angle to this PN, but most probably it is seen edge-on. VLA radio continuum observations (Zijlstra et al. 1989) are strongly supporting this view. At the wavelength 4.9 GHz, which gives the distribution of the electron gas, K3-82 appears bipolar with two brightness enhancements coinciding with the two knots in Fig. 2.

3.2. Systemic and expansion velocities

The measurements with the Fabry-Pérot spectrometer are shown in Fig. 4. The full circles represent the original measurements whereas the histograms give a Savitzky-Golay smoothing with 5 adjacent points.

The systemic bulk velocity can be determined from the Hα and [O III] measurements. Due to the symmetrical appearance of these two lines the central wavelengths will give the systemic velocity without further assumptions on geometry. The results are in very good agreement (–63.3 and –61.5 km/s for Hα and [O III], respectively). Unfortunately, the data achieved in Hβ are extremely noisy and therefore no reliable velocity can be determined from these measurements.

To determine the expansion velocity from the Hα line (Fig. 4a) we have made use of the fact that the $FWHM$ (full width half maximum) of the measured line can be expressed approximately by a quadratic sum of the expansion velocity, the $FWHM$ of the instrumental broadening, and the $FWHM$ of the thermal broadening when no splitting of the line is indicated (see, e.g. Gieseking et al. 1986, Banerjee et al. 1990, and for a discussion of this method Holzmüller et al. 1987 and Saurer 1997a). Our result is $V_{\rm exp}$ = 28.7 km/s (the Hβ line would lead to 30.5 km/s, both with an assumed temperature of ≈10 000 K).

The [O III] line (Fig. 4b) cannot be fitted using only one gaussian. Symmetrically on each side humps (maybe better: a parallel displacement of the wings) can be recognized both in the original and smoothed data. However, a multiple gaussian fit would give a more suitable result. The two smaller components can be attributed to the receding and approaching part of the shell, whereas the component at the systemic velocity is stemming from the much brighter regions of the projected ring. This result is supported by the smaller $FWHM$ of the three components. With these assumptions the expansion velocity measured in [O III] is ≈34.5 km/s.

A pronounced asymmetry can be recognized when investigating the [N II] line (Fig. 4d). We have tried to fit this profile using two gaussians. Although this fit, in particular concerning the parameters of the smaller component, might be of lower accuracy, the results achieved in this way ($V_{\rm exp} \approx 26.8$ km/s, $V_{\rm hel} \approx -66.7$ km/s) are consistent with the other lines. It seems that mainly the receding part of the shell can be seen in [N II], the approaching part can only be detected rudimentaryly. In addition, the contribution of regions with systemic bulk velocity seems to be very low in the light of [NII]. This could be an indication either for a preferential plane, seen edge on, or for a rather thin shell in [NII]. However, we have no tool to draw further conclusions by investigating the integrated light only.

All results concerning the Fabry-Pérot measurements are summarized in Table 1. The errors which are given for the velocities are formal errors of the mathematical fitting procedures. The total errors including wavelength calibration can be estimated to be smaller than ≈5 km/s (Hippelein & Weinberger 1990). The errors in absolute fluxes can be estimated to be ≈30% (using objects that have been measured more than once).

3.3. Low resolution spectroscopy

As an example, the optical spectrum of the eastern knot of K3-82 is presented in Fig. 5. For the eastern knot and the central

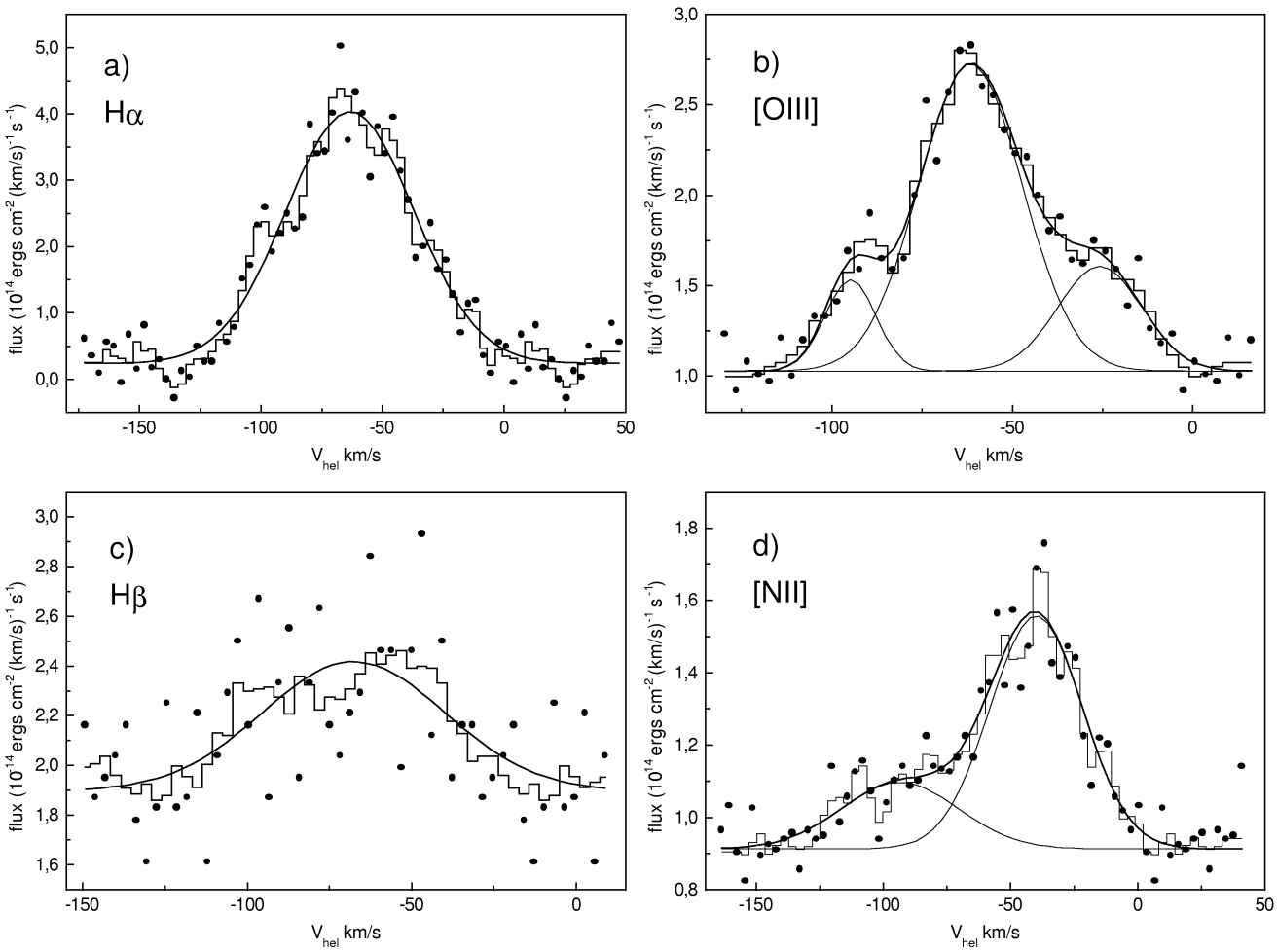

Fig. 4a–d. Fabry-Pérot measurements of K3-82

Table 1. Results of the Fabry-Pérot measurements. The second column gives the number of gaussian components used for fitting. The components according to Fig. 4 are denoted by middle, left (blueshifted component) or right (redshifted component). A colon indicates lower accuracy

line	# comp. used	comp.	$V_{\rm hel}$(comp.) (km/s)	$FWHM$ (km/s)	$V_{\rm hel}$ (km/s)	$V_{\rm exp}$ (km/s)	flux (10^{-14} ergs cm^{-2} s^{-1})	flux (total)
Hα	1	middle	–63.3±1.0	61.9±2.9	–63.3	28.7	250.0±13.1	250.0
[O III]	3	middle	–61.5±0.6	33.7±2.1	–61.5		60.9± 3.5	
	3	left	–94.8±0.9	16.6±2.2		} 34.5	8.9± 1.6	} 86.7
	3	right	–25.8±1.9	27.5±3.7			16.9± 3.1	
Hβ	1	middle	–67.7±4.9	65.3±20.0	–67.7:	30.5:	36.1±15.2	36.1
[N II]	2	left	–93.5±1.5	54.1±12.9	} –66.7:	} 26.8:	10.6± 2.9	} 40.0
	2	right	–39.9±0.5	41.9±2.7			29.4± 2.6	

region we have extracted 5″ (i.e. 5 columns), for the western knot only 2″ to avoid contamination by a star.

Because of the faintness of the [N II] 6548 line and the low resolution it was not possible to determine this line by gaussian fitting (see Fig. 1a). However, using the fit achieved for the [N II] 6548 + Hα profile, we will get an upper limit for the extinction. An approximation of a lower limit was determined by assuming the ratio [N II]6583/[N II]6548 to be $\approx$ 3 after dereddening (the values for Hα and [N II] 6548 given in Table 2 refer to this case). This procedure led to $1.7 \leq c \leq 2.1$, and we could not detect any significant differences between the three regions. For this reason a unique value (c = 1.8, see also next section) was used to deredden the line fluxes.

These line fluxes are summarized in Table 2. Listed are the element identifications, the laboratory wavelenghts (taken from Aller et al. 1996), the interstellar extinction coefficients used (see Seaton 1979 and Aller et al. 1996), the dereddened fluxes (c = 1.8) on the scale F(Hβ)=100 along with the errors. As can be

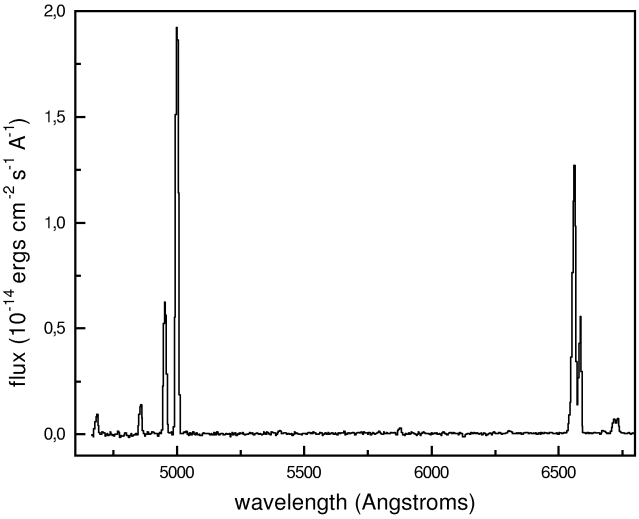

Fig. 5. Low resolution optical spectrum of the eastern knot of K3-82

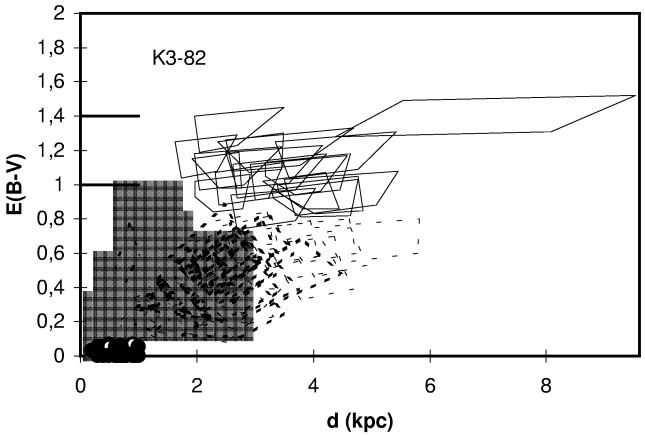

Fig. 6. The reddening–distance relation for stars within an angular radius of 10′ around K3-82. For more details of this representation and a discussion of the error areas see Saurer (1995)

seen, the Hα/Hβ ratios are consistent within the errors with the theoretical intrinsic value of 285 for Case B (see, e.g. Osterbrock 1989 and references therein). Again, the errors given in Table 2 are formal errors and originate from the fitting procedure applied to the measured lines. In the lower part of Table 2 our results for the monochromatic extinctions at Hβ are given.

The two-component gaussian fits applied to the [S II] lines, due to the low resolution, will only give rough estimates of the density (see Fig. 1b). Within the two knots the density seems to be very low ($\lessapprox 300\,\mathrm{cm}^{-3}$), whereas in the central region our result is $\approx 9000\,\mathrm{cm}^{-3}$. However, we have some doubt on the reliability of this fit for the central region, because the two lines are blended much stronger than for the two knots and almost no central trough appears in the line profile.

3.4. An attempt to determine the distance to K3-82

Our attempt to determine the distance to this PN was made by applying the "reddening–distance method" (see, e.g. Lutz (1973), Acker (1978), Kaler & Lutz (1985), Gathier et al. (1986), Martin (1994), Kerber 1996). This method is based on determining the distance to a PN by fitting its reddening into a reddening-distance diagram, usually achieved by brightness measurements of stars within a close angular vicinity of the nebula. As a fact, the errors in brightnesses, even when rather small, are leading to considerable errors within the reddening-distance plane. However, the error areas within this plane are strongly dependent on the location of the stars in the two-colour diagram. For several stars large errors in distance but small errors in reddening, and vice versa, happen to occur. In this way the determination of reliable individual distances is possible in a number of cases (see Saurer 1995, Saurer 1997b).

Our result for the reddening-distance relation in the line of sight to K3-82 is shown in Fig. 6. We have used the reddening curve $E(U-B)/E(B-V) = 0.72 + 0.05\,E(B-V)$ with the unreddened curves of the luminosity classes III and V (taken from Schmidt-Kaler 1982) and the reddening–extinction relation $R = A_V/E(B-V) = 3.2$.

In general, the thicker lines indicate higher weight, for more details of this method and a discussion of the errors see Saurer (1995). As can be seen from this figure, the extinction $E(B-V)$ seems to be smaller than ≈0.7 for distances $d \leq 2$ kpc. In the region $2\,\mathrm{kpc} \leq d \leq 4\,\mathrm{kpc}$ it increases to at least $E(B-V) \approx 0.8$.

The monochromatic extinction at Hβ deduced from our low resolution spectroscopy was $1.7 \leq c \leq 2.1$. This is in good agreement with $c = 2.0$ of Tylenda et al. (1992), who determined the extinction from Hβ and radio fluxes (Acker et al 1991, Zijlstra et al. 1989). The same authors also list $c = 1$ (very uncertain) measured from optical spectra. Sabbadin et al. (1987) gives $c = 1.5$. Our Fabry-Pérot measurements indicate $c = 1.2$, but these data are rather poor for Hβ. From this variety of results we conclude that $1.5 \leq c \leq 2.1$ should be valid with a somewhat higher weight given to lower values. This leads to $1.0 \leq E(B-V) \leq 1.4$.

Unfortunately, these values fall into a region within the reddening-distance relation which can only result in uncertain distances for two reasons. First, it is not possible to predict the reddening distance relation for $E(B-V) \geq 0.8$ and $d \geq 2.5$ kpc. It can reach a plateau at $E(B-V) \approx 1 \pm 0.2$ or increase further. Second, the data for $E(B-V) \geq 0.8$ are all of less weight, i.e. not free of ambiguities. For those reasons only a reliable minimum distance can be read off from Fig. 6: 2.5 kpc.

Because K3-82 coincides with an IRAS point source ($F(12\mu m) < 0.34$, $F(25\mu m) = 2.35$, $F(60\mu m) = 4.08$, $F(100\mu m) < 22.75$, fluxes in Jy) we cannot exclude that the measured reddening to K3-82 is partly due to internal extinction. It is hardly possible to estimate this contribution. However, even an internal extinction of $E(B-V) \approx 0.6$ (i.e. $A_V \approx 2, c \approx 0.9$) would not change the minimum distance significantly. In addition, the IRAS colours correspond to relatively cold dust (≈ 120 K, Tajitsu & Tamura 1996), and, due to its size, this PN is certainly not in the first stage of expansion

Table 2. Results of the low resolution measurements with the 1.83 m telescope on Cima Ekar. Given are the element identifications, the laboratory wavelengths, the extinction coefficients, and the dereddened fluxes for the western knot, the central part, and the eastern knot of K3-82, scaled to $F(\mathrm{H}\beta)$=100. $F(\mathrm{H}\beta)$ (uncorrected for extinction) is given in 10^{-15} ergs cm^{-2} s^{-1} Å^{-1}. The interstellar extinction correction was done by applying $F_0 = F \cdot \mathrm{dexp}(c(f(\lambda)+1))$, $c = 1.80$ for all the three parts. The errors were calculated straightforward by using the formalism of error propagation

element	λ_{lab}	$f(\lambda)$	F(west)	F(center)	F(east)
Hβ	4861.33	0.000	100.0± 14.1	100.0± 12.9	100.0± 11.6
[O III]	4958.92	-0.023	447.9± 46.3	408.7± 40.7	427.2± 35.1
[O III]	5006.84	-0.034	1394.8±159.4	1260.8±117.9	1306.5±119.1
He I	5875.67	-0.216	13.1± 3.4	0.0± 0.0	8.8± 1.9
[N II]	6548.03	-0.321	35.3± 2.5	23.6± 1.5	37.6± 2.2
Hα	6562.82	-0.323	312.5± 37.3	264.6± 24.8	296.8± 30.5
[N II]	6583.41	-0.326	106.1± 20.0	70.7± 12.2	112.7± 16.6
[S II]	6716.47	-0.343	13.7± 1.6	6.9± 1.0	17.5± 1.9
[S II]	6730.85	-0.345	11.8± 1.4	13.7± 1.7	12.4± 1.4
$F(\mathrm{H}\beta)$			2.4± 0.2	9.5± 0.6	10.8± 0.6

Table 3. The UBV values of the stars in an angular vicinity of 10′ around K3-82 used for dereddening. The error of the measurement is ≈ 0.06 mag. Star 14 turned out to be variable

#	V	$B-V$	$U-B$	#	V	$B-V$	$U-B$	#	V	$B-V$	$U-B$	#	V	$B-V$	$U-B$
1	13.77	0.27	0.16	29	14.04	0.82	0.15	57	15.07	0.77	0.51	84	14.77	0.24	0.40
2	13.53	0.50	0.15	30	15.06	0.65	0.28	58	14.71	0.40	0.16	85	13.72	0.46	0.04
3	12.64	1.13	0.63	31	14.89	0.78	0.12	59	13.14	1.32	0.89	86	15.29	0.60	0.28
4	12.89	0.71	0.25	32	13.74	0.47	0.53	60	14.69	0.86	0.18	87	13.63	0.77	0.13
5	13.00	1.47	1.18	33	14.83	0.66	0.28	61	14.71	0.78	0.40	88	14.44	0.67	0.23
6	14.51	0.99	0.20	34	14.18	0.50	0.53	62	15.37	0.55	0.30	89	14.68	0.53	0.38
7	13.85	0.86	0.27	35	14.64	0.69	0.37	63	14.70	0.70	0.19	90	14.44	0.43	0.33
8	14.61	0.63	0.31	36	14.76	0.66	0.19	64	15.40	0.57	0.19	91	14.70	0.45	0.34
9	14.89	0.65	0.18	37	15.10	0.67	0.27	65	13.13	1.13	0.88	92	13.75	0.76	0.47
10	14.45	0.53	0.09	38	15.41	0.99	0.28	66	14.13	0.80	0.34	93	13.26	1.54	1.05
11	13.73	0.78	0.39	39	15.32	1.13	0.14	67	13.53	0.39	0.40	94	14.40	0.86	0.16
12	14.66	0.87	0.30	40	13.32	1.64	1.03	68	14.80	0.49	0.19	95	14.27	0.50	0.45
13	14.73	0.62	0.33	41	13.41	0.56	0.10	69	14.00	0.29	0.47	96	15.15	0.52	0.33
14				42	14.88	0.63	0.38	70	13.16	0.22	0.31	97	14.45	0.79	0.46
15	13.58	1.15	0.69	43	13.81	0.80	0.22	71	13.95	0.69	0.05	98	13.51	0.71	0.40
16	13.23	0.43	0.25	44	14.18	0.91	0.28	72	14.61	0.56	0.52	99	14.68	0.57	0.45
17	13.98	0.46	0.35	45	13.50	0.64	0.08	73	13.11	1.39	0.95	100	13.27	0.83	0.31
18	12.70	0.89	0.56	46	14.55	0.84	0.36	74	14.30	0.66	0.27	101	14.86	0.79	0.20
19	14.79	1.04	0.54	47	15.01	0.88	0.22	75	13.77	0.98	0.26	102	12.42	0.63	0.45
20	13.90	0.86	0.54	48	13.43	0.48	0.22	76	14.42	0.76	0.29	103	14.44	1.12	0.33
21	13.58	0.48	0.37	49	14.40	0.88	0.45	77	14.29	0.97	0.50	104	14.40	0.92	0.47
22	14.23	0.51	0.47	50	15.05	0.70	0.27	78	14.84	0.57	0.25	105	14.91	1.01	0.35
23	14.43	0.86	0.33	51	14.86	0.70	0.52	79	13.84	0.90	0.16	106	14.13	0.27	0.25
24	14.54	0.58	0.35	52	13.30	0.62	0.58	80	14.95	0.62	0.36	107	14.61	0.72	0.32
25	14.47	0.83	0.27	53	14.63	1.05	0.48	81	14.88	0.76	0.15	108	14.78	0.63	0.47
26	14.49	0.52	0.31	54	13.44	0.62	0.16	82	15.01	0.31	0.46	109	14.99	0.71	0.37
27	13.43	0.96	0.60	55	12.70	0.55	0.04	83	14.70	0.74	0.12	110	14.68	0.62	0.11
28	14.45	0.91	0.19	56	14.11	0.84	0.67								

(rich in dust). Therefore the value of $E(B-V)$ seems to be mainly caused by interstellar absorption (and hence one single mean value was assumed for the three regions).

Statistically derived distances for K3-82 can be found in Tajitsu & Tamura (1996): 3.2 kpc, Zhang (1995): 3.73 kpc, Van de Steene & Zijlstra (1994): 3.25 kpc, and Cahn et al. (1992): 2.68 kpc.

Accepting a mean distance of 3.2 kpc, the linear size of the shell would be 0.16 pc and its kinematical age ≈ 5000 years. An estimation of the visual brightness of the central star from the red and blue Palomar Observatory Sky Prints gives $19 \leq m_V \leq 20.5$ ($m_B = 19.5$ can be found in Kohoutek 1972). With the total Hβ-flux (Table 1) and the adopted extinction the hydrogen-Zanstra temperature of the central star is 85 000 ± 20 000 K and its radius can be determined to be $0.02 \pm 0.01\ \mathrm{R}_\odot$. Finally, the

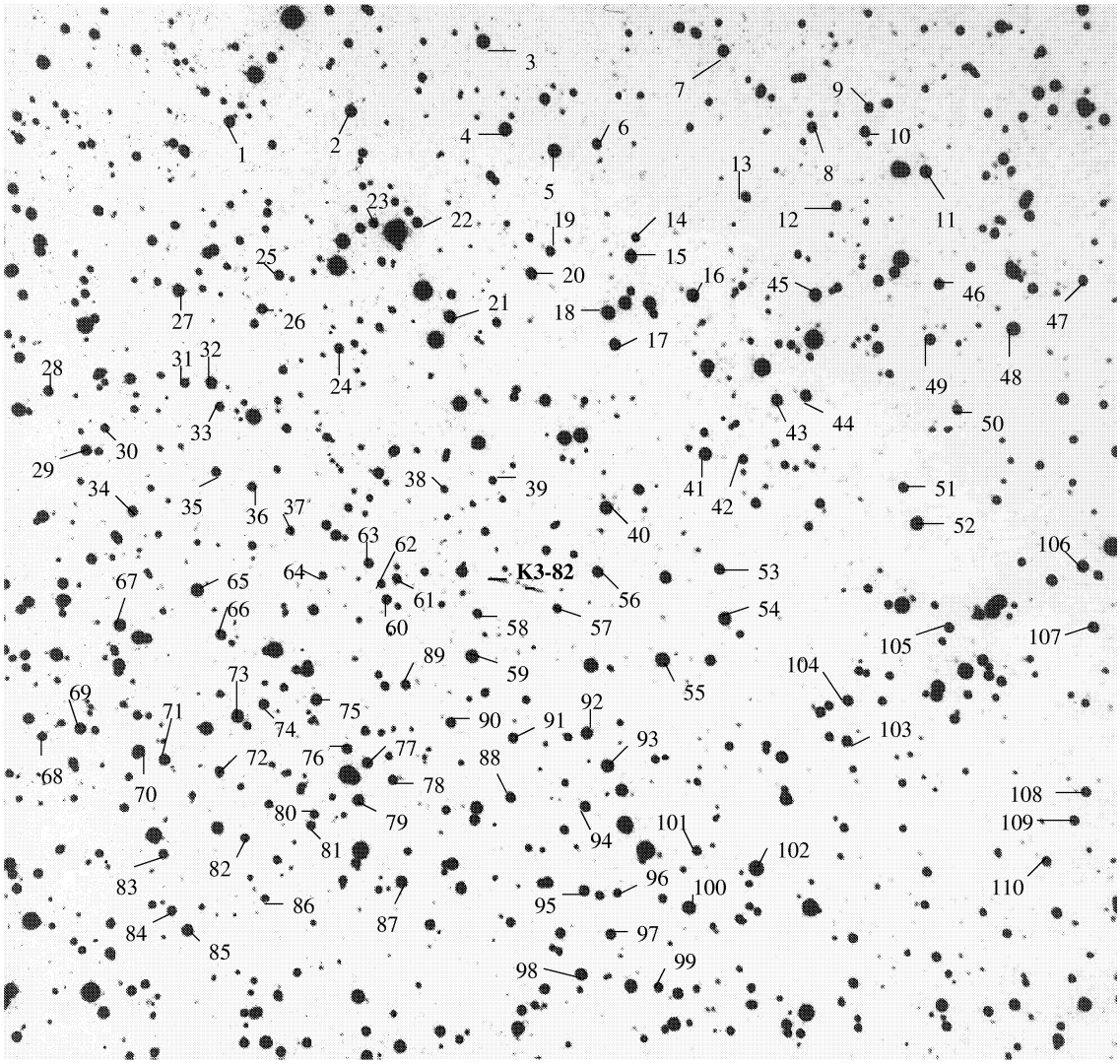

Fig. 7. Finding chart for the stars around K3-82 used for dereddening. The number of each star corresponds to the number in Table 3. The size of the image is $26' \times 26'$. North is to the top and East to the left.

position of this star within the Hertzsprung-Russel diagram is given by $L/L_{\odot} \approx 20$ and $\lg T \approx 4.9$.

4. Conclusions

The planetary nebula K3-82 was investigated by means of high resolution Fabry-Pérot and optical low resolution spectroscopy, along with direct imaging in Gunn-red. This PN turned out to be a highly symmetrical nebula. The most remarkable features of K3-82 are two point-symmetrically arranged knots which appear both in the radio continuum and in the Hα+[N II] direct image. They represent either concentrated emission regions within the shell or the edge-brightened parts of an incomplete torus-like structure. The expansion velocity of the shell does not differ significantly from the average (Weinberger 1989). All in all, it seems to be worthwhile to investigate this PN in more detail.

Acknowledgements. The author is grateful to Prof. R. Weinberger for helpful discussions and carefully reading the manuscript. We also would like to thank for observing time at the 1.2 m and the 2.2 m telescopes of the German-Spanish Calar Alto Observatory, and at the 1.83 m telescope of the University of Padova on Cima Ekar, Asiago, Italy. For their helpfulness special thanks go to the staff of these observatories. We also would like to thank U. Boorgest, J. Schramm, H. Hippelein, and R. Weinberger who have made some observations used in this paper during their observing runs. Special thanks go to C. Zanin who provided us with the optical spectrum of K3-82. This work was supported financially by the "Fonds zur Förderung der wissenschaftlichen Forschung", project P 5708 (travel costs), by the "Österreichische Forschungsgemeinschaft", project 06/1006 (travel costs), and by the "Jubiläumsfonds der österreichischen Nationalbank", project 4713 (computer facilities).

Appendix A: UBV brightnesses of the program stars

In Table 3 we present the photographic brightnesses of the stars used for dereddening.

Appendix B: finding chart for the program stars

Fig. 7 is a finding chart for the stars used for dereddening.

References

Acker A., 1978, A&AS 33, 367
Acker A., Stenholm B., Tylenda R., Raytchev B., 1991, A&AS 90, 89
Acker A., Ochsenbein F., Stenholm B., Tylenda R., Marcout J., Schohn C., 1992, Strasbourg-ESO Catalogue of Galactic Planetary Nebulae, ESO
Aller L.H., Hyung S., Feibelman W.A., 1996, PASP 108, 488
Banerjee D.P.K., Anandarao B.G., Jain S.K., Mallik D.C.V., 1990, A&A 240, 137
Cahn J.H., Kaler J.B., Stanghellini L., 1992, A&AS 94, 399
Chevalier R.A., in Asymmetrical Planetary Nebulae, ed. A. Harpaz & N. Soker, Ann. Israel Phys. Soc., 11, 240
Corradi R.L.M., Schwarz H.E., 1995, A&A 293, 871
Dorfi E.A., Höfner S, 1996, A&A 313, 605
Ebner E.J., 1973, doctoral thesis, Innsbruck, Austria
Frank A., Balick B., Icke V., Mellema G., 1993, ApJ 404, L25
Gathier R., Pottasch S.R., Pel J.W., 1986, A&A 157, 171
Gieseking F., Hippelein H., Weinberger R., 1986, A&A 156, 101
Hippelein H., Münch G., 1981, Mitt. Astron. Ges. 54, 193
Hippelein H., 1984, Fabry-Pérot-Interferometer, Benutzeranleitung,
Hippelein H., Weinberger R., 1990, A&A 232, 129
Hoag A.A., Johnson H.L., Iriarte B., Mitchell R.I., Hallam K.L., Sharpless S., 1961, Publication of the United States Naval Observatory, Second Series, Vol. XVII, Part VII
Holzmüller G., Huemer G., Saurer, W., 1987, Mitt. Astron. Ges. 70, 339
Iben Jr. I., 1995, Phys. Rep. 250, 1
Icke V., Balick B., Frank A., 1992, A&A 253, 224
Kaler J.B., Lutz J.H., 1985, PASP 97, 700
Kerber F., 1996, doctoral thesis, Innsbruck, Austria
Kohoutek L., 1972, A&A 16, 291
Kwok S., Purton C.R., Fitzgerald M.P., 1978, ApJ 219, L125
Livio M., 1995, in Asymmetrical Planetary Nebulae, ed. A. Harpaz & N. Soker, Ann. Israel Phys. Soc., 11, 51
Lutz J.H., 1973, ApJ 181,135
Manchado A., Guerrero M.A., Stanghellini L., Serra-Ricart M., 1996b, The IAC Morphological Catalog of Northern Galactic Planetary Nebulae, Instituto de Astrofísica de Canarias
Martin W., 1994, A&A 281, 526
Mellema G., Eulderink F., Icke V., 1991, A&A 252, 718
Osterbrock D.E., 1989, Astrophysics of Gaseous Nebulae and Active Galactic Nuclei, University Science Books, Mill Valley, California, ISBN 0-935702-22-9
Pascoli G., 1995, Ap&SS 234, 281
Sabbadin F., Falomo R., Ortolani S., 1987, A&AS 67, 541
Saurer W., Pfitscher K., Weinberger R., Hartl H., 1992, A&AS 93, 553
Saurer W., 1995, A&A 297, 261
Saurer W., 1997a, A&A in press
Saurer W., 1997b, MNRAS submitted
Schmidt-Kaler Th., 1982, in: Landolt-Börnstein, New Series, Group VI, Vol.2, Subvol. b
Seaton M.J., 1979, MNRAS 187, 73p
Stanghellini L., Corradi R.L.M., Schwarz H.E., 1993, A&A 276, 463
Tajitsu A., Tamura S., 1996, preprint
Van de Steene G.C., Zijlstra A.A., 1994, A&AS 108, 485
Tylenda R., Acker A., Stenholm B., Köppen J., 1992, A&AS 95, 337
Weinberger R., 1989, A&AS 78, 301
Zhang C.Y., 1995, ApJS 98, 659
Zijlstra A.A., Pottasch S.R., Bignell C., 1989, A&AS 79, 329

This article was processed by the author using Springer-Verlag LaTeX A&A style file *L-AA* version 3.